Theor Chem Account (2007) 118:607–622
DOI 10.1007/s00214-007-0349-8

REGULAR ARTICLE

Relativistic calculations on the ground and excited states of AgH and AuH in cylindrical harmonic confinement

John M. H. Lo · Mariusz Klobukowski

Received: 14 December 2006 / Accepted: 17 February 2007 / Published online: 11 July 2007

Abstract The relativistic ground and low-lying excited state potential energy curves of AgH and AuH in the presence of a cylindrical harmonic confining potential were calculated using the multi-state multi-reference perturbation theory with the spin-free no-pair Hamiltonian obtained via the third-order Douglas–Kroll transformation, incorporated with the full two-electron Breit–Pauli spin–orbit operator. The spectroscopic parameters were obtained for both the scalar- and quasi-relativistic potentials. The spin–orbit coupling constants were calculated for several strengths of the confining potential, and the effects of the applied potential on the coupling constants were analyzed using configuration interaction.

Keywords Spin–orbit effects · Silver hydride · Gold hydride · Confinement effects

1 Introduction

Calculations of molecular properties of compounds containing heavy transition-metal elements is one of the most challenging issues in computational quantum chemistry. On one hand, these calculations can provide information related to the development and applications of transition metal compounds in the areas such as materials science and catalysis [1]. On the other hand, the accuracy of the calculations involving heavy transition metals is very sensitive to the methods employed. Since the number of electrons is large and the electronic states are often quasi-degenerate, sophisticated methods including the extensive treatment of electron correlation effects are mandatory. In addition, the large relativistic effects experienced by both core and valence electrons often lead to failures of conventional non-relativistic quantum chemistry methods.

There are several promising approaches of incorporating the relativistic effects in quantum chemical calculations. The simplest one involves the use of pseudopotentials that greatly reduce the number of electrons explicitly considered in the computations by removing the chemically inert core electrons and replacing them with a potential operator [2]. Since the generation of pseudopotential parameters depends on the reference orbitals and energies from all-electron calculations, a relativistic pseudopotential may be produced by utilizing the reference from the Dirac–Hartree–Fock (DHF) atomic calculation [3]. A proper all-electron approach is to perform molecular calculations using directly the Dirac–Coulomb Hamiltonian. However, it suffers from a deficiency that the two-electron interaction term is not Lorentz-invariant. This problem can be partially solved by introducing the frequency-independent Breit operator to the two-electron Coulomb term [4], leading to the Dirac–Coulomb–Breit (DCB) Hamiltonian. The resulting DHF equation is very complicated and the four-component wavefunctions are very difficult to interpret. Therefore, several schemes have been proposed to decouple the large component (which corresponds to the electronic solution) and the small component (which corresponds to the positronic solution) of the DHF solutions [5–8].

Among these two-component methods, the Douglas–Kroll (DK) transformation [9], further developed by Hess and

This paper is dedicated to Serafín Fraga—colleague, mentor, and friend.

J. M. H. Lo · M. Klobukowski (✉)
Department of Chemistry, University of Alberta,
Edmonton, AB, T6G 2G2 Canada
e-mail: mariusz.klobukowski@ualberta.ca

J. M. H. Lo
e-mail: jmlo@ualberta.ca

coworkers [10], is the one most successfully applied in relativistic molecular calculations. This method stems from the free-particle Foldy–Wouthuysen transformation where a unitary transformation is carried out on the Dirac Hamiltonian in the external field. It follows that subsequent unitary transformations are to be performed in order to eliminate the odd terms of arbitrary orders in the external potential to avoid the problem of singularity. The DKn method (where n is the order of transformation) has been tested in a number of atomic and molecular calculations of heavy metal compounds and produced satisfactory results [11–13]. In the present study of coinage metal hydrides, the third-order Douglas–Kroll transformation was chosen to recover the relativistic energy contributions.

The spin–orbit effects in atoms and molecules were concisely and elegantly reviewed by Fraga and Malli almost 40 years ago [14]. In the present work, the effects of spin–orbit coupling were included in a perturbative fashion using the full one- and two-electron Breit–Pauli Hamiltonian [15].

Two coinage metal hydrides, AgH and AuH, were investigated in the present study. These two molecules have been often studied because they serve as excellent examples of the profound effects of relativity. For instance, the strong relativistic effect experienced by the 6s electrons of Au atom causes the anomalously high first ionization potential and the unusual ordering of the low-lying excited states [16]. Both non-relativistic and relativistic molecular calculations have been carried out for these compounds, using extended all-electron basis sets and effective potentials (for a summary, see [17]). Nevertheless, the majority of these studies was focused only on the ground state properties, such as r_e, ω_e and D_e, and only a few were devoted to the excited states [18,19].

In the present study the ground and excited state properties of AgH and AuH confined in a cylindrical harmonic potential were computed. Studies of confinement effects have become a major research topic [20], and confining potentials have been shown to be very useful models in the studies of plasma [21], external magnetic field [22], and quantum dots [23]. The model of harmonic confining potential has been recently applied to several molecular systems [24–26], and the basic understanding of the confinement effects in terms of orbital response has been obtained. Therefore, the aim of the present work was to investigate the combined effects of external confinement and relativity on the molecular properties, in particular the spin–orbit coupling constants, of AgH and AuH.

2 Computational details

An excellent review of the Douglas–Kroll (or Douglas–Kroll–Hess) transformation may be found in the series of publications by Hess et al. [27,28] and Hirao et al. [29,30]. In the present work, no transformation on the two-electron operators was considered, and the instantaneous non-relativistic Coulomb two-electron operator was used instead

$$\mathcal{H}(\mathbf{r}_i, \mathbf{r}_j) = \sum_{i<j}^{N} \frac{e^2}{r_{ij}}. \tag{1}$$

However, it is expected that the influence of this approximation will be minimal [31].

The confining potential used in the present study is an electrostatic repulsion operator acting solely on electrons. It is defined, for an N-electron system, as a sum of one-electron terms:

$$\mathcal{W}(\mathbf{r}_1, \mathbf{r}_2, \ldots \mathbf{r}_N) = \sum_{i=1}^{N} w(\mathbf{r}_i) \tag{2}$$

in which $\mathbf{r}_i$ represents the coordinates of the i-th electron. The one-electron term can, in general, be expressed as a power series in the electronic coordinates

$$w(\mathbf{r}_i) = \frac{1}{2}\left[\omega_x^{n_x+1}(x_i - b_x)^{2n_x} + \omega_y^{n_y+1}(y_i - b_y)^{2n_y} + \omega_z^{n_z+1}(z_i - b_z)^{2n_z}\right] \tag{3}$$

where $\mathbf{r}_i = \{x_i, y_i, z_i\}$. Geometry of the potential is defined by choosing suitable values of the power (n_x, n_y, n_z) and the center (b_x, b_y, b_z) of the potential. In frequent use is the harmonic oscillator potential ($n_x = n_y = n_z = 1$). In all the following calculations a cylindrical harmonic potential was adopted, in which $n_x = n_y = 1$ and $n_z = 0$, with $\omega_x = \omega_y = \omega$ and $\omega_z = 0$. The axis of the potential was assumed to overlap the molecular axis of the diatomic molecules; hence, the origin of the potential may be defined at the origin of the coordinate system, i.e., $b_x = b_y = b_z = 0$. The resulting confining potential is thus represented by

$$\mathcal{W}(\mathbf{r}_1, \mathbf{r}_2, \ldots \mathbf{r}_N) = \sum_{i=1}^{N} \frac{1}{2}\left[\omega_x^2 x_i^2 + \omega_y^2 y_i^2\right] \tag{4}$$

and the total spin-free Hamiltonian is obtained by adding Eqs. (1) and (4) to the DK3 Hamiltonian.

In order to treat the electron correlation effects we used the recently developed spin–orbit second-order quasi-degenerate perturbation theory (SO-MCQDPT2) [32]. This method makes use of the orbitals generated in the complete active space self-consistent field (CASSCF) calculations to obtain the zeroth-order states for the spin-free Hamiltonian. The spin–orbit coupling is calculated using the full microscopic Breit-Pauli spin–orbit Hamiltonian [33] which gives rise to the off-diagonal coupling terms between the zeroth-order states in the effective Hamiltonian. Subsequently, the second-order perturbation is performed on both the spin-free and spin–orbit parts, and the resulting spin-mixed states

(expressed as linear combinations of the zeroth-order states) are produced via the diagonalization of the perturbed Hamiltonian [34]. This approach ensures the inclusion of the scalar relativistic effects from the spin-free wavefunctions obtained from the Douglas–Kroll Hamiltonian, and the proper treatment of the avoided crossing between states of the same symmetry [32].

All-electron basis sets were used for all atoms. The primitive basis set for Ag is the $24s17p12d4f3g$ set developed by Witek et al. [35], with exponents optimized at the second-order Douglas–Kroll and averaged coupled-pair functional levels for the balanced description of the ^2S, ^2D and ^2P states. This basis set is contracted to $13s10p8d4f3g$ by contracting the tightest $14s10p6d$ to $3s3p2d$. In the present work, the three g-functions were dropped, yielding the final $13s10p8d4f$ basis set. For Au, the first-order polarized $21s17p11d9f$ basis set of Sadlej was used [36]. This basis set was designed for the relativistic calculations of molecular electric properties in the Douglas–Kroll no-pair approximation. The set of $13s10p7d$ with the largest exponents are contracted to $5s4p3d$, leaving all the other s, p and d primitives uncontracted. For the f-functions they are contracted in the 3, 2, 2, 2 pattern. These contraction schemes lead to the contracted $13s11p7d4f$ Gaussian basis set. In both cases, the Dunning's cc-pVQZ basis set was used for H [37]. Spherical harmonic Gaussians were used in all calculations.

The orbitals required in the SO-MCQDPT2 calculations for AgH and AuH were generated using the CASSCF method, with the active space for both AgH and AuH consisting of ten orbitals: $1s$ for H, $4d$, $5s$ and $5p$ for Ag and $5d$, $6s$ and $6p$ for Au; in both cases 12 electrons were explicitly correlated. In order to perform the spin–orbit calculations, one common set of molecular orbitals was used to describe all the zeroth-order states. This set of orbitals was obtained from a state-averaged CASSCF over the lowest 18 electronic states which correlate to the first four dissociation channels. In the subsequent perturbation calculations, 18 core orbitals, corresponding to $[Ar]3d4s4p$ orbitals, were frozen for AgH while 34 core orbitals composed of $[Kr]4d4f5s5p$ orbitals were uncorrelated for AuH. To eliminate the intruder states in the effective Hamiltonian, the intruder state avoidance (ISA) scheme [38] was used in which the energy denominators around the poles are shifted. The parameters of 0.02 for the spin-free terms and 0.1 for the spin–orbit terms were used as suggested by Witek et al. [38].

The SO-MCQDPT2 spectroscopic parameters for several electronic states of AgH and AuH were calculated using the Dunham's fourth order polynomial [39]. All the CASSCF and SO-MCQDPT2 calculations were carried out using the program GAMESS-US [40] which has been modified to include the features for the confinement effects.

Table 1 Spectroscopic constants of the singlet states of AgH (r_e in Å, ν_e in cm^{-1}, T_e in eV). Experimental data from [42–44]

State		r_e	ν_e	T_e
$1\,^1\Sigma^+$	This work	1.5635	2024	0.00
	[19]	1.620	1901	0.00
	[35]	1.564	2073	0.00
	Experiment	1.618	1760	0.00
$2\,^1\Sigma^+$	This work	1.7503	1166	4.03
	[19]	1.604	1807	3.64
	[35]	1.717	1422	3.99
	Experiment	1.665	1664	3.71
$3\,^1\Sigma^+$	This work	2.0669	1126	6.73
	[19]	2.201	925	6.87
	[35]	2.093	1026	6.72
	Experiment	1.862	1220	5.52
$4\,^1\Sigma^+$	This work	1.7035	2682	7.80
	[35]	4.596	433	7.22
$1\,^1\Delta$	This work	1.7743	1303	6.31
	[19]	1.790	1310	5.90
$1\,^1\Pi$	This work	1.5763	1654	6.19
	[19]	1.842	1240	5.65
	Experiment	1.61	1589	5.11
$2\,^1\Pi$	This work	1.8119	1271	6.32
	[19]	1.643	1720	5.87
	Experiment	1.80	845	5.79

3 Results and discussion

3.1 Spin–orbit coupling without confinement

In the SO-MCQDPT2 calculations of AgH in C_{2v} point group symmetry, 18 states (eight A_1, two A_2, four B_1, and four B_2) have been calculated, corresponding to the following twelve electronic states for diatomics in $C_{\infty v}$ symmetry: four $^1\Sigma^+$, one $^1\Delta$, two $^1\Pi$, two $^3\Sigma^+$, one $^3\Delta$, and two $^3\Pi$. These states, except for the $4\,^1\Sigma^+$ which correlates to the asymptote of $Ag(^2S, 6s) + H(^2S)$, arise from the $Ag(^2S) + H(^2S)$, $Ag(^2P) + H(^2S)$, and $Ag(^2D) + H(^2S)$ atomic states and comprise the first three dissociation channels. The computed excitation energies for $Ag(^2S) \rightarrow Ag(^2P)$ and $Ag(^2S) \rightarrow Ag(^2D)$ are 3.794 and 4.051 eV, respectively, which agree fairly well with the values of 3.740 and 3.971 eV recently measured by Fourier-transform spectrometry [41]. The systematic overestimation of the excitation energies could be a consequence of using the CASSCF orbitals optimized for both the ground and excited states of AgH. The spectroscopic constants for these states are summarized in Tables 1 and 2. In general, the performance of the SO-MCQDPT2 is far from excellent. For the ground and first several low-lying states the agreement

Table 2 Spectroscopic constants of the triplet states of AgH (r_e in Å, ν_e in cm^{-1}, T_e in eV). Experimental data from [42–44]

State		r_e	ν_e	T_e
$2\,^3\Sigma^+$	This work	1.9511	1,326	6.17
	[19]	1.953	1,516	6.26
$1\,^3\Delta$	This work	1.7726	1,327	6.20
	[19]	1.795	1,276	5.78
	Experiment	1.875		
$1\,^3\Pi$	This work	1.5994	1,530	5.59
	[19]	1.582	1,751	5.38
	[35]	1.594	1,620	5.49
	Experiment	1.64	1,450	5.17
$2\,^3\Pi$	This work	1.7954	1,397	6.07
	[19]	1.814	1,329	5.39
	[35]	1.845	1,198	6.01
	Experiment	1.85		

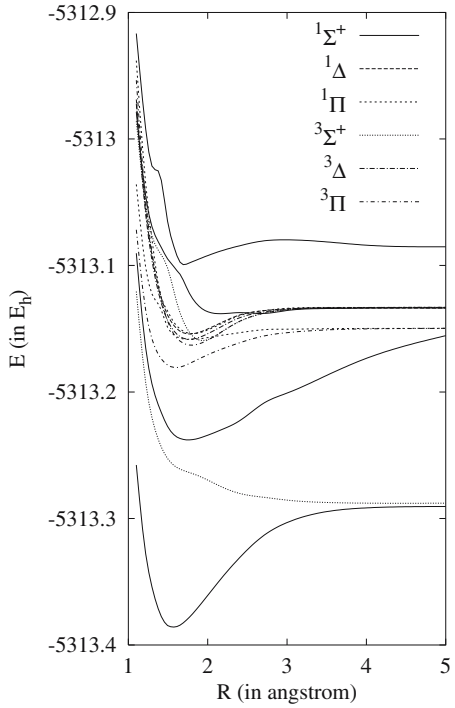

Fig. 1 Relativistic spin-free MCQDPT2 potential energy curves for the selected low-lying states of AgH in free space

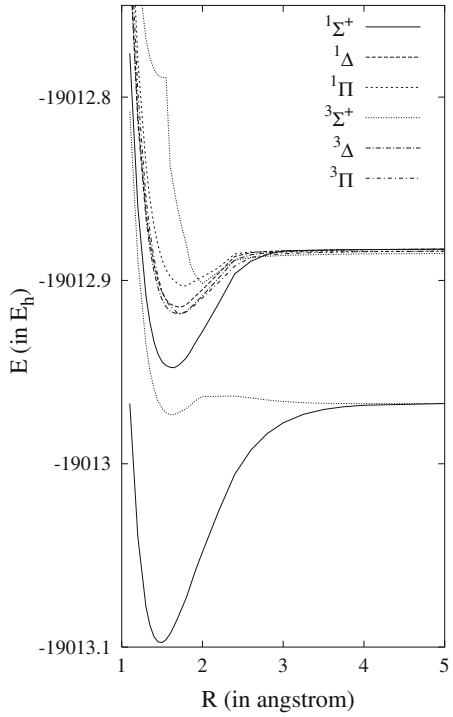

Fig. 2 Relativistic spin-free MCQDPT2 potential energy curves for the selected low-lying states of AuH in free space

with the available experimental data is acceptable; however, the situation becomes worse for higher excited states. For instance, the discrepancy in r_e is 0.2 Å for the $3\,^1\Sigma^+$ state. This is not unexpected, since the orbitals utilized in the SO-MCQDPT2 calculations for different states were simultaneously optimized at CASSCF level for states of Σ, Π and Δ symmetries with different spins, which, consequently, might not be able to describe well the high-lying states. Similar results have also been observed in the SO-MCQDPT2 studies of AgH using both state-averaged and state-specific CASSCF orbitals [35]: the spectroscopic parameters obtained for the potentials computed using the state-averaged orbitals show a larger deviation from the experiment (Fig. 1).

Another possible source of error arises from the insufficient s-space in the Ag basis set. Although utilizing a smaller $18s8p5d2f$ basis set for Ag, the MRMP2 calculations of Witek et al. yielded $r_e = 1.620$ Å for the ground state AgH which differs from the experiment by only 0.002 Å [19].

The potential energy curves for a number of low-lying states of AuH were also calculated using SO-MCQDPT2 method in C_{2v} symmetry, and they are shown in Fig. 2. Twelve electronic states were investigated which correspond to the following eight states in diatomics: two of $^1\Sigma^+$, two of $^3\Sigma^+$, and one for each of $^1\Pi$, $^3\Pi$, $^1\Delta$ and $^3\Delta$. Spectroscopic parameters were obtained using the calculated potentials, and they are listed in Table 3. The data from Witek et al. [35] and Hess et al. [18], together with available experimental values, are also included for comparison. In general, the results of the present work agree fairly well with the available experimental and computed values, with the largest error in r_e (0.09 Å shorter) found for the $2\,^1\Sigma^+$ state.

Only two dissociation channels were studied for AuH: Au(^2S) + H(^2S) and Au(^2D) + H(^2S). Contrary to the case of AgH, where the excited Ag(^2P) lies about 0.2 eV below Ag(^2D), the first excited state of Au is ^2D, with the excitation energy of 1.74 eV [18]. The atomic calculation of Au

Table 3 Spectroscopic constants of the selected states of AuH (r_e in Å, ν_e in cm^{-1}, T_e in eV). Experimental data from [44]

State		r_e	ν_e	T_e
$1\,^1\Sigma^+$	This work	1.4942	2,480	0.00
	[35]	1.493	2,414	0.00
	[18]	1.52	2,381	0.00
	Experiment	1.5238	2,305	0.00
$2\,^1\Sigma^+$	This work	1.5864	2,118	3.71
	[35]	1.572	2,198	3.27
	[18]	1.60	2,029	3.31
	Experiment	1.673	1,670	3.43
$1\,^1\Delta$	This work	1.7116	1,335	4.77
	[35]	1.662	1,658	4.65
	[18]	1.64	1,827	4.01
$1\,^1\Pi$	This work	1.7704	1,784	5.10
	[35]	1.747	1,342	5.12
	[18]	1.73	1,492	4.37
$1\,^3\Sigma^+$	This work	1.6224	1,737	3.30
	[35]	1.654	1,715	3.31
	[18]	1.63	1,755	2.75
$2\,^3\Sigma^+$	This work	2.0312	1,568	5.12
	[35]	2.100	1,693	6.82
$1\,^3\Delta$	This work	1.7042	1,339	4.67
	[35]	1.656	1,688	4.53
	[18]	1.66	1,503	3.91
$1\,^3\Pi$	This work	1.7234	1,402	4.71
	[35]	1.700	1,598	4.64
	[18]	1.72	1,221	3.90
	Experiment	1.695	1,545	4.78

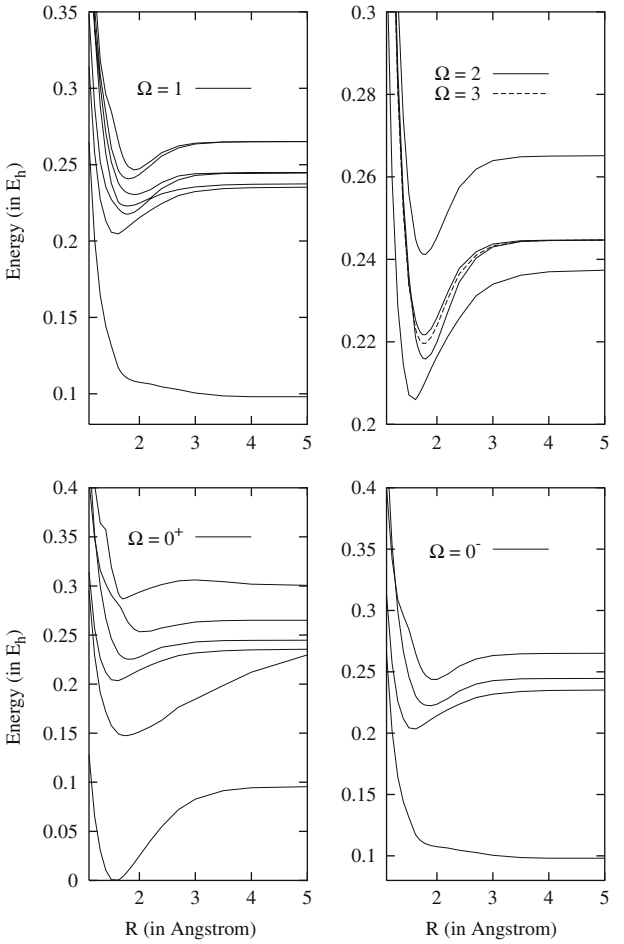

Fig. 3 Relativistic spin–orbit MCQDPT2 potential energy curves for the selected low-lying states of AgH in free space. Energies are plotted with respect to $E_{\min}$ of the 0^+(I) state

using the Sadlej's basis set at SO-MCQDPT2 level yielded the excitation energy of 1.69 eV which differs from the experiment by only 0.05 eV. However, the value obtained in the molecular calculations for AuH at $R = 5$ Å was about 2.1 eV, closer to experiment than the value of 2.4 eV, estimated from the work of Witek et al. [19].

The first dissociation channel includes the ground $^1\Sigma^+$ and $1\,^3\Sigma^+$ states, both arising from the ionic Au^+H^- pair at small R and covalent $Au(5d^{10}6s^1)$ + $H(1s)$ configuration at large R. The ionic character for these states near the equilibrium region was verified by the Mulliken population analysis, which assigned the charge of −0.3 to the H atom. This value is consistent with the value reported by McLean [45] and Hess et al. [18]. This configuration mixing leads to the presence of a local maximum in the $1\,^3\Sigma^+$ state and the corresponding minimum which lies 0.17 eV above the dissociation limit.

The second dissociation channel consists of six electronic states: $2\,^{1,3}\Sigma^+$, $1\,^{1,3}\Pi$ and $1\,^{1,3}\Delta$. Except for the $2\,^1\Sigma^+$ which possesses a relatively deep potential curve, all the other states are only weakly bound with respect to the dissociation products of $Au(^2D)$ + $H(^2S)$. Similarly to the second and third channels of AgH, this phenomenon may be understood in terms of the destabilization of Au $5d$ orbitals that weakens the overlap with the H $1s$ orbital, and thus reduces the bonding interaction.

When the spin–orbit coupling is included in the calculations, the $\Lambda - S$ scheme for the state symmetry assignment is no longer valid, and the $\omega - \omega$ scheme was used. According to the double group analysis, the following relativistic state symmetries will be obtained from the non-relativistic classifications of diatomic electronic states: 0^+ from $^1\Sigma^+$ and $^3\Pi$; 0^- from $^3\Sigma^+$ and $^3\Pi$; 1 from $^{1,3}\Pi$ and $^{1,3}\Delta$; 2 from $^3\Pi$ and $^{1,3}\Delta$ and 3 from $^3\Delta$ [46]. Accordingly, 22 relativistic states will be generated from the 12 electronic states of AgH while 15 relativistic states are derived from the 8 electronic states of AuH.

The potential energy curves for the ground and excited states of AgH and AuH, calculated including the spin–orbit coupling interaction, are plotted in Figures 3 and 4,

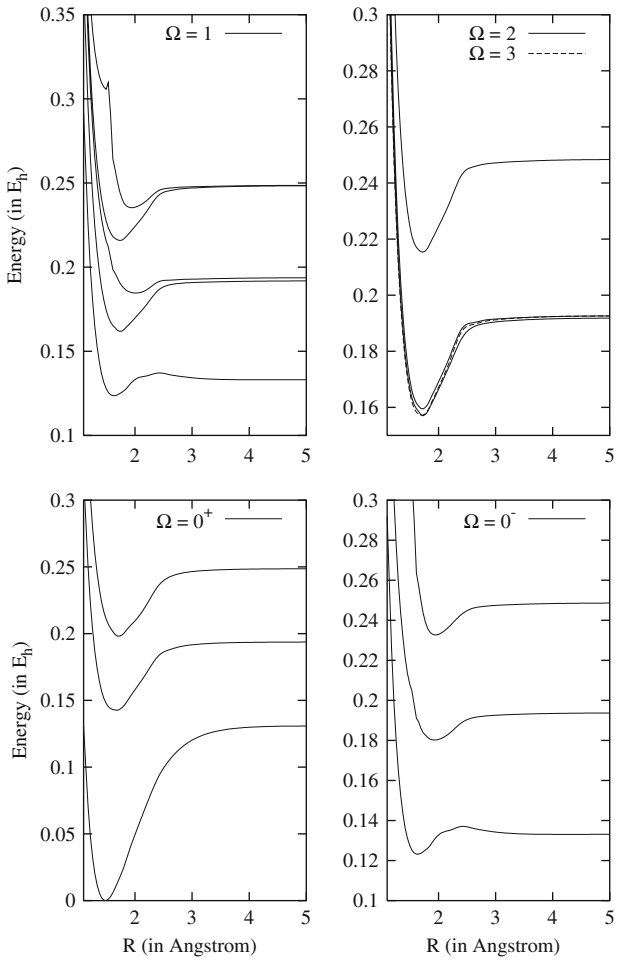

Fig. 4 Relativistic spin–orbit MCQDPT2 potential energy curves for the selected low-lying states of AuH in free space. Energies are plotted with respect to $E_{\min}$ of the 0^+(I) state

respectively. Spectroscopic parameters were evaluated using these potentials, and they are compared with the available experimental data in Tables 4 and 5.

The first three dissociation channels for the excited states of AgH in the spin-free calculations split into five channels due to the spin–orbit coupling. While the first channel does not split because of the non-degenerate Ag($^2S_{1/2}$) state, the other two give rise to Ag($^2P_{1/2}$) + H($^2S_{1/2}$) and Ag($^2P_{3/2}$) + H($^2S_{1/2}$), and Ag($^2D_{5/2}$) + H($^2S_{1/2}$) and Ag($^2D_{3/2}$) + H($^2S_{1/2}$), respectively. The energy differences between these limits may be used to obtain the fine structure splitting. The estimated Ag($^2S_{1/2}$ - $^2P_{1/2}$) and Ag($^2D_{5/2}$ − $^2D_{3/2}$) splittings are 3.73 and 0.56 eV which agree with the experimental values within 2% of error [41]. However, the value for the Ag($^2P_{1/2}$ − $^2P_{3/2}$) splitting determined by this method is only 0.06 eV which is 48% smaller than the experimental data (0.1142 eV). Atomic SO-MCQDPT2 calculations of Ag employing the same basis set increased the spin–orbit splitting to 0.1061 eV, but the discrepancy is still remarkably large (∼10%). There are two possible reasons to account for the observed large error in the spin–orbit splitting for the P term. On one hand, the imbalanced spin–orbit interaction and electron correlations treatment of the atomic Ag p-orbitals during the state-averaged MCSCF calculations causes the spin-polarization [2] that stabilizes the $P_{3/2}$ component more than the $P_{1/2}$ component, leading to the reduced Ag($^2P_{1/2}$ - $^2P_{3/2}$) splitting. On the other hand, in the computer code implementation, the neglect of the screening effect by the contracted Ag 5s orbital provides extra contribution to the core-valence correlation on the $5p_{3/2}$ orbital which diminishes the spin–orbit splitting of the P state [30].

Table 4 Spectroscopic constants of the spin–orbit states of AgH (r_e in Å, ν_e in cm^{-1}, T_e in eV)

State		r_e	ν_e	T_e
0^+(I)	Calc.	1.5614	2,078	0.00
	Expt.	1.618	1,760	0.00
0^+(II)	Calc.	1.7549	1,194	4.03
	Expt.	1.665	1,490	3.71
0^+(III)	Calc.	1.5745	1,661	5.54
	Expt.	1.64	1,450	5.17
0^+(IV)	Calc.	1.8284	1,251	6.14
	Expt.	1.86	1,089	5.52
0^+(V)	Calc.	2.0669	1,126	6.89
	Expt.	2.10		
0^+(VI)	Calc.	1.7134	2,575	7.82
0^-(II)	Calc.	1.5717	1,673	5.54
	Expt.	1.64	1,450	5.17
0^-(III)	Calc.	1.8645	1,138	6.06
0^-(IV)	Calc.	1.9511	1,326	6.64
1(II)	Calc.	1.5763	1,654	5.58
	Expt.	1.61	1,589	5.11
1(III)	Calc.	1.7956	1,321	5.93
	Expt.	1.875		
1(IV)	Calc.	1.7822	882	6.08
	Expt.	1.85		
1(V)	Calc.	1.9116	907	6.28
	Expt.	1.80	845	5.79
1(VI)	Calc.	1.8120	1,282	6.56
	Expt.	1.82		
1(VII)	Calc.	1.9181	1,382	6.72
2(I)	Calc.	1.5785	1,650	5.61
	Expt.	1.64	1,450	5.17
2(II)	Calc.	1.7917	1,379	5.89
2(III)	Calc.	1.7726	1,327	6.05
2(IV)	Calc.	1.7746	1,330	6.58
3(I)	Calc.	1.7709	1,337	5.99

Experimental data from [44]

Table 5 Spectroscopic constants of the spin–orbit states of AuH (r_e in Å, ν_e in cm^{-1}, T_e in eV)

State		r_e	ν_e	T_e
0^+(I)	Calc.	1.4827	2,504	0.00
	Expt.	1.524	2,305	0.00
0^+(II)	Calc.	1.6692	1,621	3.88
	Expt.	1.673	1,670	3.43
0^+(III)	Calc.	1.7165	2,008	5.40
	Expt.	1.695	1,545	4.78
0^-(I)	Calc.	1.6324	1,573	3.34
0^-(II)	Calc.	1.9327	784	4.91
0^-(III)	Calc.	1.9436	1,244	6.34
	Expt.	1.68	1,229	5.32
1(I)	Calc.	1.6304	1,579	3.34
1(II)	Calc.	1.7453	2,074	4.41
1(III)	Calc.	2.0386	715	5.03
1(IV)	Calc.	1.7376	1,619	5.88
	Expt.	1.728	1,076	5.32
1(V)	Calc.	1.9388	1,186	6.41
2(I)	Calc.	1.7327	2,052	4.28
2(II)	Calc.	1.7237	1,754	4.34
2(III)	Calc.	1.7228	1,633	5.86
	Expt.	1.745	1,020	5.30
3(I)	Calc.	1.7032	1,335	4.28

Experimental data from [44]

The potential energy curves including spin–orbit coupling in the excited states of AgH are very similar to the corresponding spin-free potentials. For the 0^+ and 0^- states the values of r_e differ by about 0.05 Å, and ν_e by 100–200 cm^{-1}. These rather small changes are due to the large separation of the $^1\Sigma^+$, $^3\Sigma^+$ and $^3\Pi$ states which leads to a weak coupling. Nonetheless, a complicated situation occurs in the 1 states, where a prominent avoided crossing due to spin–orbit coupling exists between the 1(III) and 1(IV) states. These two states originate from the non-relativistic $1\,^1\Pi$ and $2\,^3\Pi$ states which cross at 2.1 Å due to the spin selection rule. At the point of avoided crossing the mixing of $^1\Pi$ and $^3\Pi$ states was detected. For small R the 1(III) state is well described by $^1\Pi$ while the 1(IV) state is dominated by $^3\Pi$; for large R, however, these contributions interchange, and the $^3\Pi$ configuration becomes the major one for the 1(III) state yet the 1(IV) possesses the $^1\Pi$ character. Similarly to the 1(III) and 1(IV) states, the higher 1 states are also mixtures of the closely spaced $^{1,3}\Pi$ and $^{1,3}\Delta$. Their equilibrium bond lengths and vibrational constants are largely dependent of the dominant configurations of these states in the region. An exception is the 1(V) state, which may be classified as the $2\,^1\Pi$ state, whose r_e is shifted by 0.1 Å due to the interaction with the $^3\Sigma^+$ states.

An interesting feature was found between the 2(III) and 3(I) states where the 3(I) potential curve lies only 450 cm^{-1} below that for the 2(III) state at r_e. Both states arise from the $1\,^3\Delta$ state which has the inverted splitting due to the spin–orbit effect. The calculated spin–orbit coupling constant for the $^3\Delta$ state is 2,520 cm^{-1} at r_e. However, the strong second-order coupling with the $^1\Delta$ state, which comprises the 2(IV) state, lowers the $\Omega = 2$ component of the $^3\Delta$ state by 1,776 cm^{-1}. This perturbation, together with the coupling with the $^3\Pi$ state, significantly lowers the 2(III) state and reduces the energy separation between the 2(III) and 3(I) states.

In comparison with AgH, the influence of spin–orbit interaction on the spectroscopic parameters and electronic structure of AuH molecule is more pronounced. This strong effect is clearly manifested in the order of the electronic states of Au and in their fine structure splitting constants. In contrast to the case of Ag, where the ^2P states are slightly lower in energy than the ^2D states, the ^2D and ^2P states of Au are well separated, and the ^2D states are in fact lower than the ^2P states by 3.20 eV [44], when averaged over all the fine structure components. This is a direct consequence of the relativistic contraction of Au 6s orbital which favors the $5d \rightarrow 6s$ over the $6s \rightarrow 6p$ excitations. In addition to different ordering of atomic states, the $^2D_{5/2}$ $-^2D_{3/2}$ splitting is three times larger than the corresponding value in Ag. The computed value in the present work is 1.494 eV, in very good agreement with the experiment (1.522 eV); however, the calculated $^2S_{1/2}$ - $^2D_{5/2}$ splitting is 1.712 eV which is 51% larger than the value deduced by Ehrhardt and Davis [47]. Because the spin-polarization effect is small for d-shell orbitals, the over-estimated $^2S_{1/2}$ - $^2D_{5/2}$ gap could be possibly due to the excessive stabilization of the 6s-orbital by the use of the atomic charge of 79 for Au, instead of an effective nuclear charge.

The first relativistic 0^+(I) state of AuH, which is derived from the $1\,^1\Sigma^+$ state, was not much affected when the spin–orbit coupling was considered because of the wide separation from the other 0^+ states. The 3(I) state resembles the parent $^3\Delta$ state in terms of r_e and ν_e since only one 3 state was calculated. A small increase in the binding energy for the 0^+(I) state was found; this effect is expected, since the spin–orbit coupling induces the decrease of the overlap-related kinetic energy at r_e [48]. A similar effect was seen in the 3(I) state, whose binding energy increased by 0.06 eV, compared to that for the $^3\Pi$ state.

In general, the effect of spin–orbit interaction on r_e for these states is small, except for the 0^-(II) and 1(III) states where the bond lengths were stretched by 0.21 and 0.30 Å, respectively. While the vibrational constants normally increase due to the relativistic effects, the calculated values of ν_e for some states of AuH decreased when spin–orbit interaction was added. Furthermore, the magnitude of changes

in ν_e was large, ranging from 200 to 600 cm^{-1}. It was also observed that the states arising from the second dissociation channel, i.e., Au(^2D) + H(^2S), were more susceptible to the influence of the spin–orbit interaction. In contrast to AgH, the relativistic states of AuH with $\Omega = 1$ or 2 contain large contributions from $^{1,3}\Pi$ and $^{1,3}\Delta$ states. At the SO-MCQDPT2 level, the off-diagonal spin–orbit coupling constants between the Π and Δ states and between Δ and Δ states are approximately 3,000 and 5,000 cm^{-1}, respectively. Therefore, their potential curves are strongly distorted from the corresponding non-relativistic potentials, giving rise to relatively large and irregular changes in r_e and ν_e.

The effects of spin–orbit interaction on the two states are unique: their bond lengths were stretched by 0.01–0.02 Å but the vibrational constants were raised by 400 to 600 cm^{-1}. The 2(I) state is characterized almost exclusively by the $^3\Pi$ state while the 2(II) and 2(III) states are composed of the $^1\Delta$ and $^3\Delta$ states. These states possess very strong ionic character of Au^+H^- occurring as a result of the charge transfer from Au 5d orbitals to H 1s orbital at r_e. Hence, the spin–orbit coupling destabilizes these states and lifts their potential curves at the region around r_e. Simultaneously, the covalent $1s_H 5d_\sigma 6s_\sigma^2$ contribution, that intervenes and leads these states to the correct dissociation limit of Au(^2D) + H(^2S), is stabilized at large R. In consequence, the resulting potential curves for these states are deepened and shifted towards larger R.

3.2 Effects of confinement on spin–orbit coupling

In order to investigate the combined effects of relativity and external confining potentials on the structural and electronic properties of AgH and AuH, the SO-MCQDPT2 calculations with Eq. (4) have been performed. Several values of the confinement parameters ω were used: 0.025, 0.050, 0.075 and 0.100 au, and both spin-free and spin–orbit potential energy curves for the low-lying excited states of these molecules were computed. In order to better describe the electron density distorted by the harmonic electrostatic potential, a set of $1s1p1d$ basis functions with the exponent of $\omega/2$ were utilized and located at mid-bond position. Previous studies have demonstrated that the use of these so-called confinement functions can yield more realistic molecular orbitals and energy levels [49].

Generally, the confining potential enhances electron density between the nuclei, and leads to a stronger bonding interaction, a shorter bond length, and a larger vibrational constant. However, a complicated situation is observed in AgH where a substantial mixing of configurations occurred when the confining potential was applied, as illustrated in Tables 6 and 7.

The ground state of AgH, which is essentially characterized by the covalent Ag 5s and H 1s interaction, is mixed with the Ag $4d_{z^2}$ configuration when the confining potential is turned on. In consequence, the bonding orbital is elongated, giving rise to an increased r_e and a smaller ν_e. The $1\,^3\Sigma^+$ state remains unbound regardless the strength of the applied potential. However, a small plateau starts to appear at about 2.0 Å, possibly due to the confinement-induced relative sta-

Table 6 Spectroscopic constants of the singlet states of AgH with confinement (r_e in Å, ν_e in cm^{-1}, T_e in eV)

State		ω				
		0.000	0.025	0.050	0.075	0.100
$1\,^1\Sigma^+$	r_e	1.5635	1.5596	1.5680	1.5825	1.5904
	ν_e	2,024	2,237	1,939	1,968	1,923
$2\,^1\Sigma^+$	r_e	1.7503	1.7599	1.7329	1.7201	1.6884
	ν_e	1,166	1,298	1,269	1,266	1,546
	T_e	4.03	4.01	3.94	3.89	3.85
$3\,^1\Sigma^+$	r_e	2.0669	2.1416	2.1334	2.1284	2.1237
	ν_e	1,126	814	824	861	870
	T_e	6.73	6.76	6.77	6.80	6.87
$4\,^1\Sigma^+$	r_e	1.7035	1.6407	1.6522	1.6468	1.8590
	ν_e	2,682	2,917	898	1,378	1,383
	T_e	7.80	8.09	8.50	8.95	9.05
$1\,^1\Delta$	r_e	1.7743	1.7717	1.7669	1.7600	1.7495
	ν_e	1,303	1,316	1,339	1,369	1,436
	T_e	6.31	6.34	6.33	6.36	6.40
$1\,^1\Pi$	r_e	1.5763	1.7125	1.7672	1.7890	1.7856
	ν_e	841	911	1151	1308	1419
	T_e	6.19	6.14	6.28	6.37	6.45
$2\,^1\Pi$	r_e	1.8119	1.8464	1.8440	1.8126	1.7829
	ν_e	1,271	1,136	894	753	750
	T_e	6.32	6.47	6.58	6.81	7.15

Table 7 Spectroscopic constants of the triplet states of AgH in confinement (r_e in Å, ν_e in cm^{-1}, T_e in eV)

State		ω				
		0.000	0.025	0.050	0.075	0.100
$2\,^3\Sigma^+$	r_e	1.9511	2.0420	2.0199	2.0088	1.9919
	ν_e	1,326	1,022	1,160	1,203	1,250
	T_e	6.17	6.46	6.48	6.52	6.60
$1\,^3\Delta$	r_e	1.7726	1.7690	1.7651	1.7595	1.7513
	ν_e	1,327	1,346	1,367	1,394	1,462
	T_e	6.20	6.22	6.21	6.22	6.25
$1\,^3\Pi$	r_e	1.5994	1.5490	1.4957	1.5673	1.7736
	ν_e	1,530	2,101	3,521	1,721	1,513
	T_e	5.59	5.62	5.79	6.10	6.15
$2\,^3\Pi$	r_e	1.7954	1.7918	1.7890	1.6932	1.5914
	ν_e	1,397	1,395	1,430	2,298	2,497
	T_e	6.07	6.09	6.09	6.17	6.45

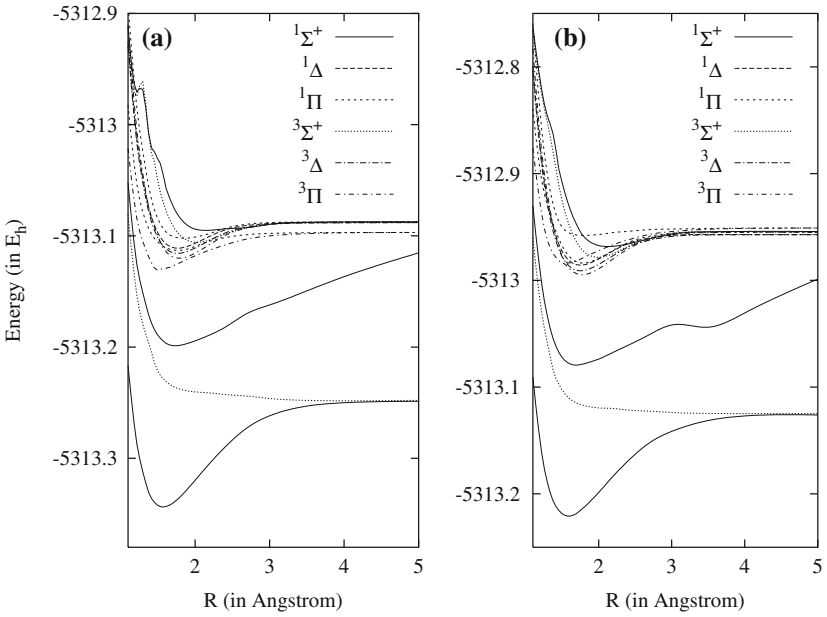

Fig. 5 Relativistic spin-free potential energy curves for the selected low-lying states of confined AgH molecule. **a** $\omega = 0.050$ au, **b** $\omega = 0.100$ au

bility of Ag $5p_z$ orbital over the Ag $5s$ orbital: contribution from the more stable Ag $5p_z$ lowers the $1\,^3\Sigma^+$ potential at small R. Evidence is found in its T_e, measured at the r_e of the ground state of AgH, which decreases from 3.47 eV for $\omega = 0.00$–3.04 eV for $\omega = 0.10$ au.

Figure 5 shows that under the influence of the harmonic confining potential the second and third dissociation channels gradually merge and split into several new channels. This phenomenon is ascribed to the complex multiplet splitting of the quasi-degenerate Ag(^2P) and Ag(^2D) states. The axially-symmetric geometry of the applied potential removes the degeneracy within the d- and p-subshells; in a confinement of cylindrical symmetry the orbitals that spread along the molecular bond axis are less destabilized compared to the ones perpendicular to the axis. Therefore, the p-subshell splits into two subsets $\{p_z\}$ and $\{p_x, p_y\}$ while the d-subshell splits into $\{d_{xy}, d_{x^2-y^2}\}$, $\{d_{z^2}\}$, and $\{d_{yz}, d_{xz}\}$. The resulting new ordering of the atomic energy levels of Ag leads to a very complicated excited state potentials of AgH which are difficult to interpret.

A remarkable change for the confined AgH molecule is that the $2\,^1\Sigma^+$ potential curve departs from the second and third channels with increasing ω, which is reflected in its T_e, which is decreasing from 4.03 eV to 3.85 eV when ω increases to 0.10 au. Concurrently, a local minimum appears at 3.5 Å which is formed due to the lowering of the ionic Ag^+H^- potential at intermediate R. The depth of this minimum is about 465 cm^{-1}, for $\omega = 0.10$ au.; vibrational level calculations reveal that this local minimum is capable of accommodating two vibrational levels, and gives rise to the discontinuity on the Birge-Sponer plot (Fig. 6).

Both the $^{1,3}\Delta$ states respond to the confining potential in a typical way: their equilibrium bond distances shorten in a stronger applied potential. As these states are formed by the $4d_\delta \rightarrow 5s$ excitation of Ag, this behavior may be understood in terms of the distorted $4d_\delta$ orbitals along the molecular axis that favours the bonding interaction with the H $1s$ orbital. The change of r_e is accompanied by the increasing ν_e, which implies stronger bonding and thus steeper potential curves for the Δ states.

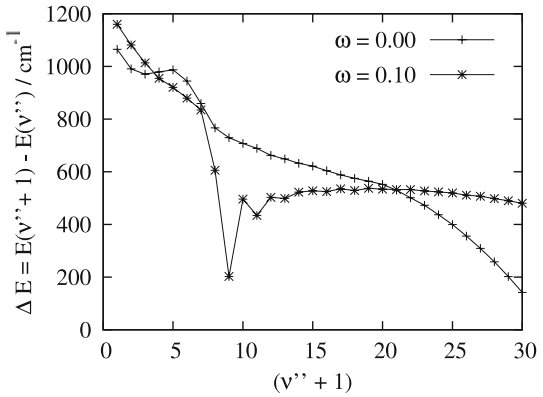

Fig. 6 The Birge-Sponer plot for the $1\,^1\Sigma^+ \leftrightarrow 2\,^1\Sigma^+$ emission of AgH

The picture for the Π states is intricate, as r_e and ν_e of these states do not vary monotonically in the presence of the confining potential. The $1\,^{1,3}\Pi$ states are first compressed when a small potential is exerted; when the strength of potential exceeds 0.05 au their bonds start to stretch very rapidly. However, the opposite trend is observed for the $2\,^1\Pi$ state, while the $2\,^3\Pi$ state exhibits the same behavior as the Δ states. These unusual variations may be rationalized in terms of the orbital responses to the external confinement.

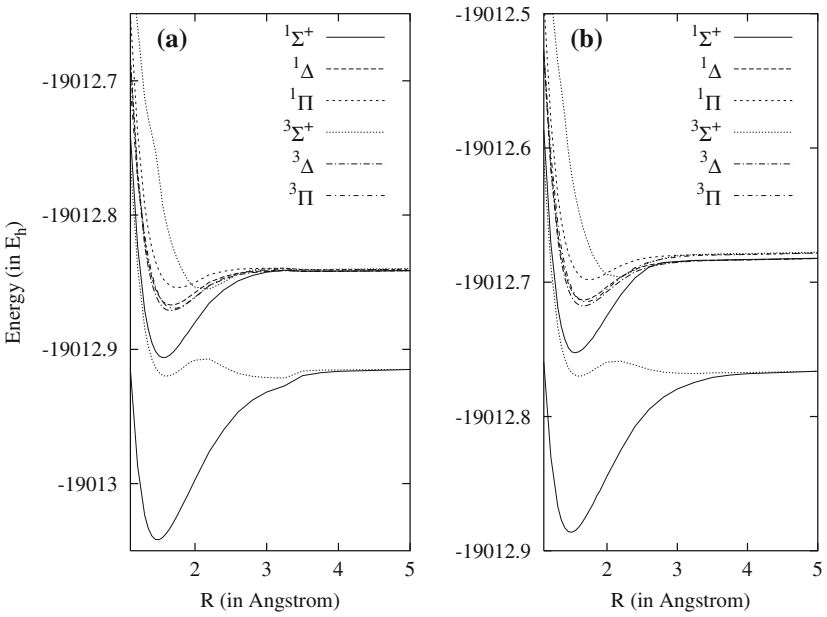

Fig. 7 Relativistic spin-free potential energy curves for the selected low-lying states of confined AuH molecule. **a** $\omega = 0.050$ au, **b** $\omega = 0.100$ au

As the $^{1,3}\Pi$ states arise from the $4d_\pi \rightarrow 5s$ excitation of Ag, the deformation of the $4d_\pi$ orbitals of Ag due to the cylindrical confining potential enhances their π-interaction with the H $1s$ orbital, thus strengthening the Π states and reducing r_e. On the other hand, the centripetal compression on the $5p_\pi$ orbitals of Ag leads to the angular distortion of the orbital towards the molecular axis and the increase in r_e of the $2\,^{1,3}\Pi$ states which are dominated by the Ag($5p_z$) + H($1s$) bonding character. For $\omega > 0.05$ au, the avoided crossing between the $^1\Pi$ states vanishes, while a new avoided crossing appears between the $^3\Pi$ states, and these interactions result in the marked distortion of the potential curves, and hence r_e and ν_e, of these states.

The effects of spatial confinement on AuH, in contrast to the case of AgH, are rather simple, as illustrated in Fig. 7. Again, the dissociation channel leading to the asymptotes of Au(^2D) + H(^2S) splits into channels corresponding to the $\{d_{xy}, d_{x^2-y^2}\}$, $\{d_{z^2}\}$ and $\{d_{yz}, d_{xz}\}$ sets. The d-subshell splitting for AuH is slightly smaller than that of AgH because of the more diffuse character of the $5d$ orbitals compared to the more contracted $4d$ counterparts in Ag. Another difference between these systems is that the entanglement of the second and third channels of the confined AgH is not found in AuH. The states that constitute the second channel remain fairly separated even at $\omega = 0.10$ au. In addition, an interesting feature in AuH is observed: the excitation energies T_e for different low-lying states of AuH are hardly affected by the confining potential, the biggest change in T_e being merely 0.17 eV for the $2\,^1\Sigma^+$ state.

The ground state geometry of AuH does not change significantly when the confining potential is applied. The

Table 8 Spectroscopic constants of the selected states of AuH in confinement (r_e in Å, ν_e in cm^{-1}, T_e in eV)

State		ω				
		0.000	0.025	0.050	0.075	0.100
$1\,^1\Sigma^+$	r_e	1.4942	1.4790	1.4783	1.4806	1.4849
	ν_e	2,480	2,512	2,479	2,425	2,354
	T_e	0.00	0.00	0.00	0.00	0.00
$2\,^1\Sigma^+$	r_e	1.5864	1.5861	1.5615	1.5595	1.5411
	ν_e	2,118	2,191	2,069	2,112	2,083
	T_e	3.71	3.81	3.69	3.67	3.64
$1\,^1\Delta$	r_e	1.7116	1.6785	1.6676	1.6722	1.6641
	ν_e	1,335	1,471	1,461	1,545	1,512
	T_e	4.77	4.72	4.76	4.74	4.70
$1\,^1\Pi$	r_e	1.7704	1.7922	1.7555	1.7534	1.7466
	ν_e	1,784	885	948	1252	1254
	T_e	5.10	5.05	5.12	5.11	5.12
$1\,^3\Sigma^+$	r_e	1.6224	1.6027	1.5912	1.6025	1.6117
	ν_e	1,737	1,682	1,695	1,842	1,697
	T_e	3.30	3.33	3.32	3.25	3.16
$2\,^3\Sigma^+$	r_e	2.0312	2.1456	2.1252	2.1375	2.1377
	ν_e	1,568	1,185	1,262	1,399	1,321
	T_e	5.12	5.02	5.07	5.08	5.15
$1\,^3\Delta$	r_e	1.7042	1.6739	1.6609	1.6673	1.6599
	ν_e	1,339	1,550	1,512	1,576	1,563
	T_e	4.67	4.62	4.65	4.62	4.58
$1\,^3\Pi$	r_e	1.7234	1.7210	1.7105	1.7113	1.6987
	ν_e	1,402	1,721	1,667	1,651	1,569
	T_e	4.71	4.65	4.69	4.68	4.67

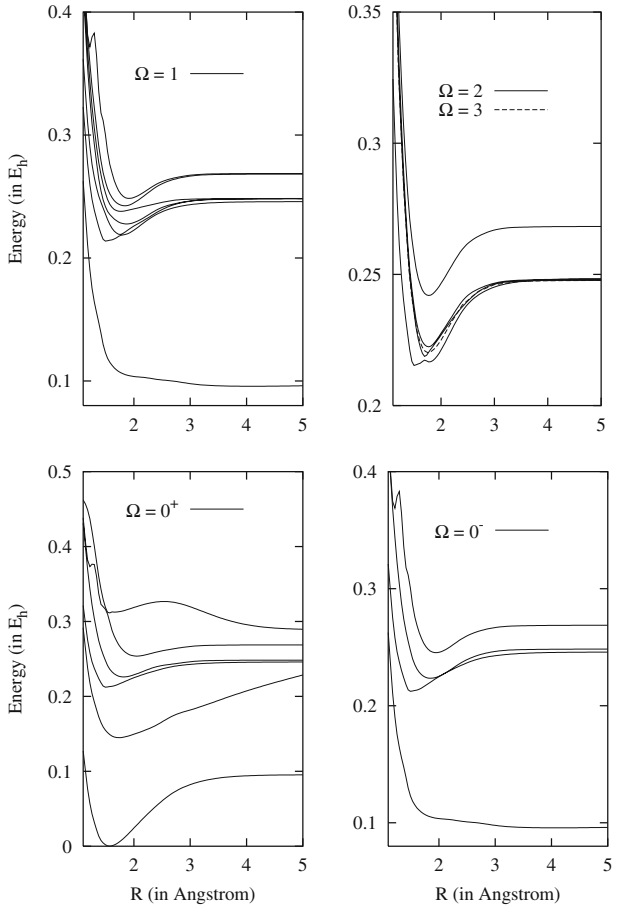

Fig. 8 Relativistic spin–orbit states of AgH in confinement for ω = 0.050 au. Energies are plotted with respect to $E_{\min}$ of the 0^+(I) state

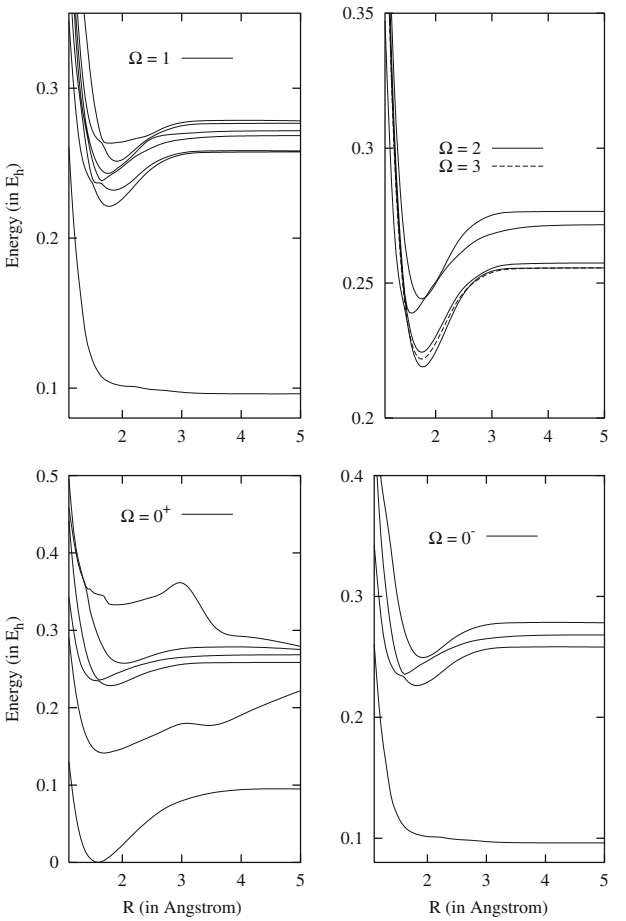

Fig. 9 Relativistic spin–orbit states of AgH in confinement for ω = 0.100 au. Energies are plotted with respect to $E_{\min}$ of the 0^+(I) state

variation in r_e is negligible, within 0.01 Å, but its binding energy is increased by almost 1 eV. This suggests that the ionic Au^+H^- configuration is more stabilized by the confining potential than the covalent Au(6s) + H(1s) configuration. This difference also causes the reduction in T_e of the $2\,^1\Sigma^+$ and $1\,^3\Sigma^+$ states, which are described by the excited Au^+H^- arising from Au $5d \rightarrow 6s$ excitation. The amplified Coulomb attraction results in the shorter bond lengths for these states.

Additional interaction is found at intermediate R, for $\omega <$ 0.05 au, where both the $1\,^1\Sigma^+$ and $1\,^3\Sigma^+$ are strongly mixed, leading to a wiggle on both potential curves. This configuration interaction induces not only the irregularity of the potential curves, but also the shift of r_e towards smaller R. The mixing of states diminishes when ω increases further until 0.10 au at which the second minimum on the $1\,^3\Sigma^+$ potential energy curve disappears, and the global minimum deepens.

Although formed via the charge transfer process from Au $5d$ orbitals to H $1s$ orbital, the $^{1,3}\Delta$ and $^{1,3}\Pi$ states exhibit slightly different behavior in confinement. The changes in the spectroscopic parameters of the Δ states caused by the applied potential are as expected: the equilibrium bond lengths decrease and the vibrational frequencies increase with increasing ω. The change of r_e for the Π states also follows the anticipated trend; however, the variations in ν_e for these two states are entirely opposite (Table 8). The anomaly for the $^1\Pi$ state is a consequence of a possible avoided crossing with higher $^1\Pi$ states that also produces a small potential barrier on the potential curve at about 3.0 Å.

The relativistic spin–orbit states of the confined AgH and AuH inherit the characteristics of the $\Lambda - S$ states from which they are derived. Figures 8 and 9 display the resulting Ω states of AgH at ω = 0.050 au and 0.100 au, respectively. The corresponding plots for AuH are depicted in Fig. 10 and 11.

The spectroscopic parameters for these states are summarized in Tables 9, 10, 11 and 12. Similarly to the spin-free case, the spin–orbit states for AgH are in general more complicated than those of AuH. Only the states that originated from the first two $^1\Sigma^+$ and $1\,^3\Sigma^+$ states are essentially unaffected by the confining potential. For $\Omega = 0^+, 0^-$, 1 and 2, the applied potential causes a numerous new avoided crossings because of the close proximity of the parent Π and Δ states.

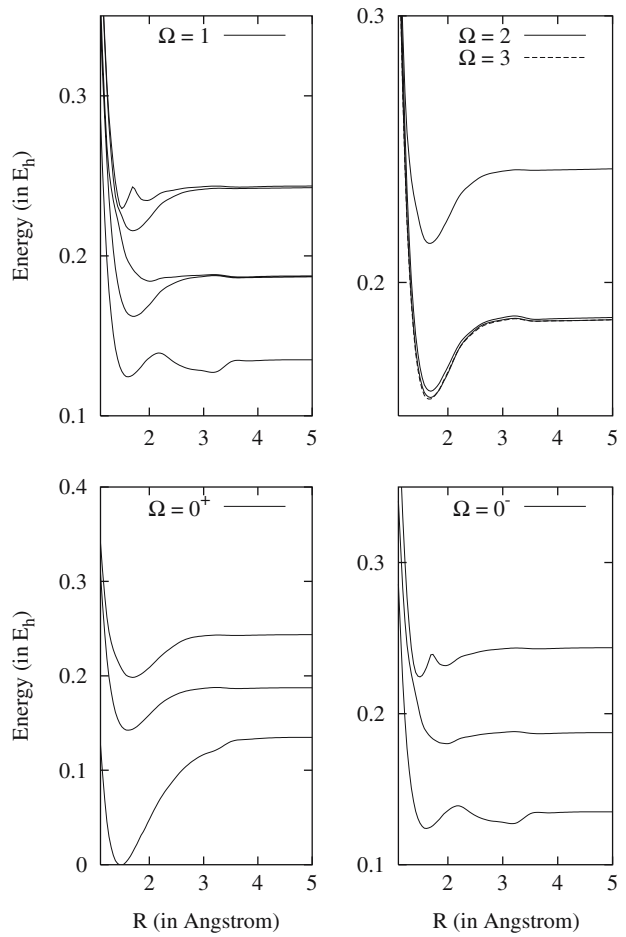

Fig. 10 Relativistic spin–orbit states of AuH in confinement for ω = 0.050 au. Energies are plotted with respect to $E_{\min}$ of the 0^+(I) state

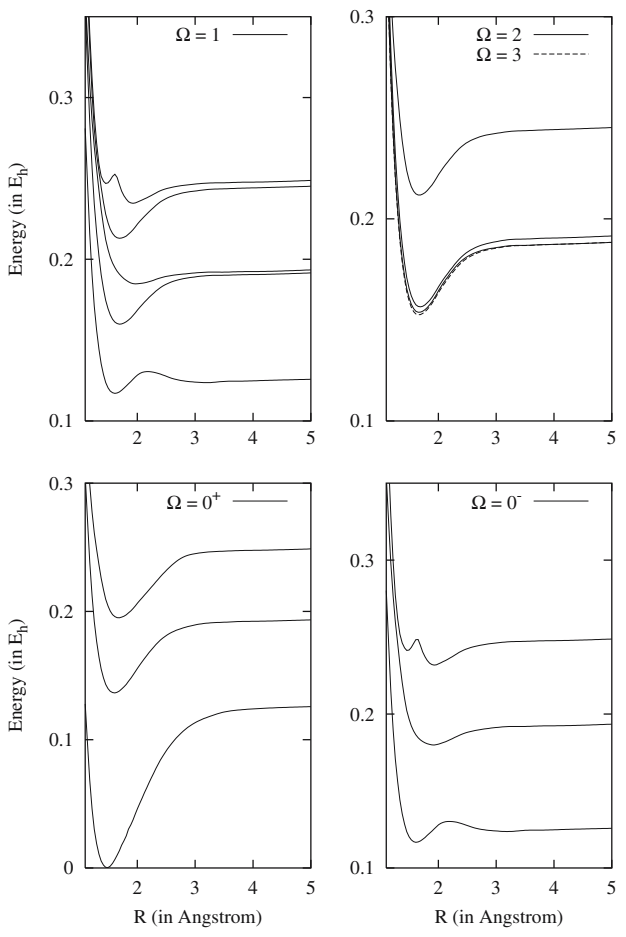

Fig. 11 Relativistic spin–orbit states of AuH in confinement for ω = 0.100 au. Energies are plotted with respect to $E_{\min}$ of the 0^+(I) state

Consequently, the r_e and ν_e values for different Ω states for different values of ω do not evolve in the same way as their parent spin-free states, and fluctuations of these quantities are observed.

Since only the first two dissociation channels were studied, the resulting spin–orbit state diagram for AuH is much simpler than that of AgH. These states, because of their rather large separations, do not interfere with each other strongly, and thus the changes of r_e and ν_e with respect to ω correlate nicely to the corresponding $\Lambda - S$ states. Even so, there are still several intriguing features that have been observed in the Ω states of the confined AuH. Due to the wiggling potential curves the 0 and 1 components of the $1\,^3\Sigma^+$ state, i.e., 0^-(I) and 1(I) states, also exhibit this character at large R. Through the spin–orbit interaction, the potential energy curves for the higher 0^- and 1 states are slightly distorted and a small potential hump is formed on the potential curves of these states. Another noticeable new feature is the double-minimum potential for the Ω states derived from the $2\,^3\Sigma^+$ state. For small values of ω, a new global minimum is formed at about 1.5 Å via the avoided crossing of the 1(V) and 1(IV) states, the latter being the 1 component of the $^3\Delta$ and $^1\Pi$ states. This minimum shifts up in energy relative to the outer minimum when ω increases. For ω exceeding 0.050 au the outer minimum becomes the global minimum again while the inner one starts disappearing. This behaviour has no counterpart in the spin-free potentials, and this feature can be considered entirely due to spin–orbit interaction.

An interesting effect of confinement is the variation of spin–orbit coupling constants with respect to the strength of the confining potential. Since the magnitude of spin–orbit coupling between two electronic states is closely related to their electronic structure, the application of an external potential which alters the wavefunction composition of different electronic states should give rise to changes of the spin–orbit coupling constants. To demonstrate this, the calculated diagonal and off-diagonal spin–orbit coupling constants for some of the excited states of AgH and AuH are plotted in Figures 12 and 13, respectively. Surprisingly, the effect of confinement on the magnitude of spin–orbit interaction is fairly small. Generally, the confining potential increases the coupling constants, but their variations with respect to the

Table 9 Spectroscopic constants of the spin–orbit 0 states of AgH in confinement (r_e in Å, ν_e in cm^{-1}, T_e in eV)

State		ω				
		0.000	0.025	0.050	0.075	0.100
0^+(I)	r_e	1.5614	1.5582	1.5679	1.5825	1.5903
	ν_e	2,078	2,095	1,940	1,968	1,923
0^+(II)	r_e	1.7549	1.7496	1.7308	1.7182	1.6874
	ν_e	1,194	1,544	1,281	1,277	1,554
	T_e	4.03	4.00	3.94	3.89	3.84
0^+(III)	r_e	1.5745	1.5481	1.5094	1.5671	1.7983
	ν_e	1,661	2,108	2,041	1,662	1,385
	T_e	5.54	5.59	5.78	6.05	6.21
0^+(IV)	r_e	1.8284	1.8247	1.8174	1.7527	1.6194
	ν_e	1,251	1,250	1,282	2,698	2,935
	T_e	6.14	6.15	6.14	6.18	6.41
0^+(V)	r_e	2.0669	2.0563	2.0491	2.0485	2.0285
	ν_e	1,126	1,146	1,150	1,223	1,151
	T_e	6.89	6.90	6.90	6.94	7.00
0^+(VI)	r_e	1.7134	1.6449	1.6371	1.6469	1.8595
	ν_e	2,575	2,643	1,324	1,379	1,368
	T_e	7.82	8.12	8.50	8.95	9.05
0^-(II)	r_e	1.5717	1.5607	1.5079	1.5685	1.8210
	ν_e	1,673	1,862	2,062	1,658	1,299
	T_e	5.54	5.60	5.78	6.05	6.15
0^-(III)	r_e	1.8645	1.8583	1.8507	1.7362	1.6162
	ν_e	1,138	1,153	1,178	2,649	2,797
	T_e	6.06	6.08	6.08	6.16	6.41
0^-(IV)	r_e	1.9511	1.9529	1.9477	1.9414	1.9244
	ν_e	1,326	1,309	1,350	1,388	1,426
	T_e	6.64	6.66	6.67	6.71	6.78

Table 10 Spectroscopic constants of the spin–orbit 1, 2, and 3 states of AgH in confinement (r_e in Å, ν_e in cm^{-1}, T_e in eV)

State		ω				
		0.000	0.025	0.050	0.075	0.100
1(II)	r_e	1.5763	1.5641	1.5120	1.7868	1.7769
	ν_e	1,654	1,857	1,976	1,386	1,468
	T_e	5.58	5.63	5,82	5.97	6.02
1(III)	r_e	1.7956	1.7953	1.7509	1.6380	1.8494
	ν_e	1,321	1,347	2,030	2,470	1,143
	T_e	5.93	5.95	5.96	6.13	6.31
1(IV)	r_e	1.7822	1.8098	1.8672	1.7927	1.6613
	ν_e	882	851	1,042	1,928	2,570
	T_e	608	6.13	6.19	6.27	6.48
1(V)	r_e	1.9116	1.8827	1.7657	1.7653	1.7582
	ν_e	907	876	1,108	1,323	1,604
	T_e	6.28	6.33	6.47	6.56	6.61
1(VI)	r_e	1.8120	1.8122	1.8400	1.9242	1.9055
	ν_e	1,282	1,293	1,254	1,291	1,454
	T_e	6.56	6.58	6.59	6.73	6.83
1(VII)	r_e	1.9181	1.9207	1.9146	1.8804	1.7911
	ν_e	1,382	1,371	1,380	1,208	821
	T_e	6.72	6.74	6.76	6.85	7.16
2(I)	r_e	1.5785	1.5520	1.5527	1.7792	1.7703
	ν_e	1,650	1,931	1,477	1,426	1,510
	T_e	5,61	5.67	5.86	5.91	5.95
2(II)	r_e	1.7917	1.7903	1.7018	1.7609	1.7520
	ν_e	1,379	1,386	2,236	1,385	1,456
	T_e	5.89	5.90	5.95	6.06	6.10
2(III)	r_e	1.7726	1.7710	1.7644	1.6300	1.5712
	ν_e	1,327	1,334	1,459	2,500	1,770
	T_e	6.05	6.05	6.05	6.17	6.50
2(IV)	r_e	1.7746	1.7730	1.7688	1.7627	1.7526
	ν_e	1,330	1,338	1,360	1,388	1,491
	T_e	6.58	6.58	6.58	6.60	6.64
3(I)	r_e	1.7709	1.7659	1.7655	1.7599	1.7516
	ν_e	1,337	1,343	1,365	1,392	1,460
	T_e	5.99	6.00	5.99	6.00	6.03

internuclear distances remain very similar compared to the unconfined cases.

More detailed information regarding the spin–orbit interaction can be extracted from these plots. For instance, Figs. 12b and 13b illustrate the computed diagonal spin–orbit coupling constants for the $^3\Delta$ state at various R. Since the $^3\Delta$ state transforms into A_1 and A_2 irreducible representations in C_{2v} symmetry, this $^3\Delta$ spin–orbit coupling constant will be dependent on both the interaction between different components of the d-shell and, in turn, the splitting of the $4d$-shell and $5d$-shell of AgH and AuH, respectively. As shown, the coupling constants increase with ω; this observation is consistent with the molecular calculations which show that the confining potential increases the fine structure splittings of $^2D_{5/2} - {}^2D_{3/2}$ of Ag and Au.

The second-order spin–orbit interactions in AgH, as revealed by Fig. 12a and c, are not significant. The applied potential only increases the coupling constants by about 100 cm^{-1}. The larger coupling constants result from the smaller energy separation between these state potential curves that gives rise to a larger second-order perturbation contribution. A noticeable drop of the coupling constant in Fig. 12a can be accounted for by strong interaction between the two $^3\Pi$ states for the confined AgH molecule. The enhanced p character in the $1\,^3\Pi$ state sharply reduces the spin–orbit interaction with the $2\,^1\Sigma^+$ which is also dominated by the Ag $5p$ character at large R.

On the other hand, the influence of the second-order spin–orbit coupling on AuH is more pronounced; in some

Table 11 Spectroscopic constants of the spin–orbit 0 states of AuH in confinement (r_e in Å, ν_e in cm^{-1}, T_e in eV)

State		ω				
		0.000	0.025	0.050	0.075	0.100
0^+(I)	r_e	1.4827	1.4482	1.4765	1.4775	1.4793
	ν_e	2,504	3,671	2,451	2,571	2,592
0^+(II)	r_e	1.6692	1.6219	1.6078	1.6086	1.6042
	ν_e	1,621	1,793	1,678	1,823	1,860
	T_e	3.88	3.93	3.89	3.81	3.71
0^+(III)	r_e	1.7165	1.6907	1.6907	1.6904	1.6752
	ν_e	2,008	1,575	1,540	1,716	1,641
	T_e	5.40	5.43	5.41	5.35	5.30
0^-(I)	r_e	1.6324	1.6169	1.6064	1.6142	1.6173
	ν_e	1,573	1,645	1,603	1,590	1,676
	T_e	3.34	3.43	3.39	3.30	3.17
0^-(II)	r_e	1.9327	2.0171	2.0549	1.9361	1.9149
	ν_e	784	1,169	884	1,087	1,077
	T_e	4.91	4.87	4.91	4.89	4.89
0^-(III)	r_e	1.9436	1.4908	1.4862	1.9362	1.9299
	ν_e	1,244	3,275	2,799	1,509	1,592
	T_e	6.34	6.02	6.11	6.30	6.30

Table 12 Spectroscopic constants of the spin–orbit 1, 2, and 3 states of AuH in confinement (r_e in Å, ν_e in cm^{-1}, T_e in eV)

State		ω				
		0.000	0.025	0.050	0.075	0.100
1(I)	r_e	1.6304	1.6153	1.6041	1.6121	1.6156
	ν_e	1,579	1,654	1,619	1,596	1,681
	T_e	3.34	3.33	3.40	3.31	3.18
1(II)	r_e	1.7453	1.7256	1.7101	1.7090	1.6976
	ν_e	2,074	1,465	1,557	1,552	1,522
	T_e	4.41	4.42	4.42	4.38	4.34
1(III)	r_e	2.0386	2.0496	2.0324	2.0003	1.9670
	ν_e	715	1,202	1,066	828	1,144
	T_e	5.03	4.97	5.02	5.01	5.02
1(IV)	r_e	1.7376	1.7097	1.6986	1.7011	1.6955
	ν_e	1,619	1,458	1,459	1,529	1,374
	T_e	5.88	5.88	5.88	5.83	5.79
1(V)	r_e	1.9388	1.5330	1.4983	1.9295	1.9237
	ν_e	1,186	4,103	3,459	1,457	1,462
	T_e	6.41	6.12	6.26	6.37	6.38
2(I)	r_e	1.7327	1.7003	1.6813	1.6814	1.6676
	ν_e	2,052	1,369	1,457	1,544	1,515
	T_e	4.28	4.29	4.28	4.23	4.18
2(II)	r_e	1.7237	1.6938	1.6846	1.6884	1.6859
	ν_e	1,754	1,490	1,519	1,636	1,575
	T_e	4.34	4.35	4.34	4.29	4.25
2(III)	r_e	1.7228	1.6879	1.6702	1.6750	1.6697
	ν_e	1,633	1,417	1,463	1,543	1,535
	T_e	5.86	5.86	5.85	5.80	5.76
3(I)	r_e	1.7032	1.6742	1.6616	1.6680	1.6595
	ν_e	1,335	1,480	1,500	1,591	1,576
	T_e	4.28	4.28	4.26	4.20	4.14

cases, the coupling constants are of the same order of magnitude as the binding energies of certain Ω states. Moreover, fluctuations in the variation of the coupling constants with respect to ω are observed, especially for $\omega \approx 0.05$ au, indicating the insufficient treatment of the double perturbation from both the confinement effects and the spin–orbit interaction. The sudden decline of the coupling constant for $\omega = 0.05$ au in, Fig. 13a, is likely caused by the configuration mixing of the $1\,^3\Sigma^+$ state, in which the additional anti-bonding character diminishes the spin–orbit interaction with the $1\,^3\Pi$ state. The $1\,^1\Pi$ and $1\,^3\Delta$ states are the major components of both the 1(III) and 1(IV) spin–orbit states. For small values of ω, a significant mixing of these states with the higher 1 states leads to the irregular shapes of these potential curves at intermediate R, and is responsible for the abnormal increment in the $^1\Pi$–$^3\Delta$ spin–orbit coupling constant (Fig. 13c).

4 Conclusions

In the studies of combined effects of relativity, electron correlation, and confinement the potential energy curves for the low-lying excited states of the coinage metal hydrides AgH and AuH were calculated using the second-order spin–orbit quasi-degenerate perturbation theory with the third-order Douglas–Kroll Hamiltonian. It was found that, under the influence of the confining potential, the spin-free channels connected to the excited dissociation products of these molecular systems split due to the symmetry restriction imposed on the p- and d-subshells of Ag and Au atoms by the cylindrical geometry of the applied potential. While the ^2P states of these atoms divide into two subsets, $\{p_z\}$ and $\{p_x, p_y\}$, the ^2D states partition into three subsets, $\{d_{z^2}\}$, $\{d_{x^2-y^2}, d_{xy}\}$ and $\{d_{xz}, d_{yz}\}$, the first two being very close in energy. An unusual feature discovered in AgH is that the second and third dissociation channels merge and redistribute when ω increases, which could possibly result from the complex re-ordering of the atomic orbitals of the confined Ag atom. The responses of different electronic states of AgH and AuH to the confining potential are not always typical; several unusual changes in r_e, ν_e, and binding energies have been noticed and are accounted for by the induced avoided crossing between the excited states.

The Ω state potential curves of these molecules have also been calculated for a several values of ω. More complica-

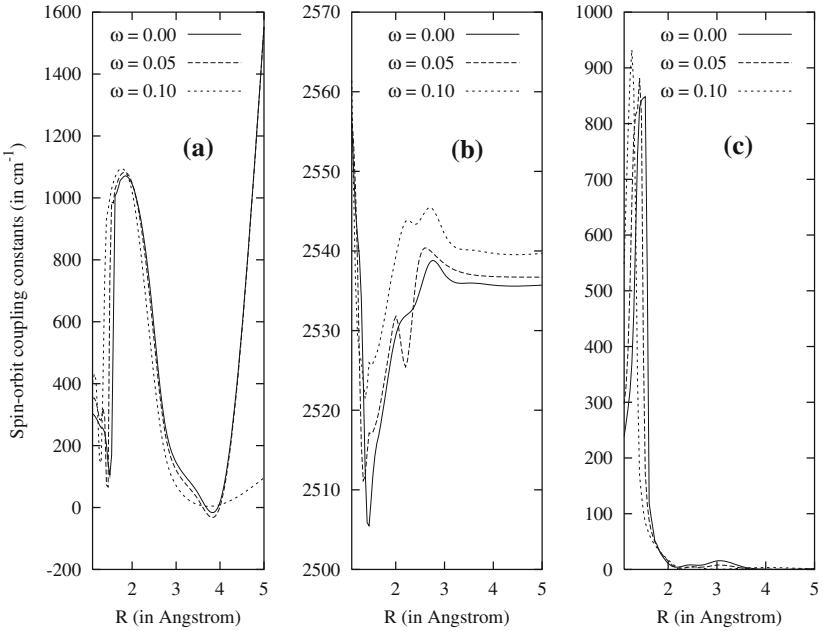

Fig. 12 Spin–orbit coupling constants for selected states of AgH in confinement. (a) $2\,^3\Sigma^+$ and $1\,^3\Pi$ states; (b) $1\,^3\Delta$ and $2\,^3\Delta$; (c) $1\,^1\Pi$ and $2\,^3\Pi$ states

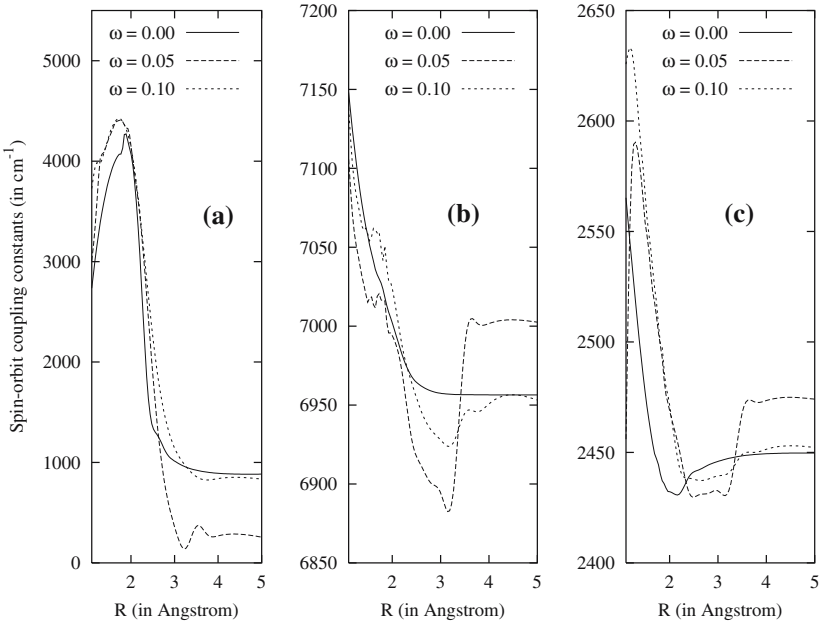

Fig. 13 Spin–orbit coupling constants for selected states of AuH in confinement. **a** $1\,^3\Sigma^+$ and $1\,^3\Pi$ states; **b** $1\,^3\Delta$ and $2\,^3\Delta$; **c** $1\,^1\Pi$ and $1\,^3\Delta$ states

ted pictures have been obtained because of the significant configuration mixing among the states possessing the same Ω components. As a result, the changes of the deduced spectroscopic parameters for these states are not in parallel to the trends observed for the spin-free counterparts. Both diagonal and off-diagonal spin–orbit coupling constants for different states of AgH and AuH molecules have been computed. It was found that the dependence of the spin–orbit coupling constants on the strengths of the confining potential is very small. Instead, the configuration mixing in the excited state wavefunctions plays a more important role in determining the resultant magnitude of the spin–orbit interactions.

Acknowledgments The authors want to acknowledge the financial support provided by the Natural Science and Engineering Research Council of Canada in forms of PGS-B Scholarship (to JL) and Research Grant (to MK), and the computer time by the Computing and

Network Services of University of Alberta. The insightful discussions with Drs. J. Karwowski and A. J. Sadlej are highly appreciated. The authors are indebted to Dr. H. Witek for providing a valuable guidance on the spin–orbit coupling calculations using the GAMESS-US program.

One of the authors (MK) would like to express his gratitude to Serafín Fraga for 27 years of scientific collaboration, generous support, and personal friendship. His skeptical optimism and humour made difficult times much easier to bear. The breadth and depth of his scientific interests will remain an inspiration.

References

1. Greenwood NN, Earnshaw A (2002) Chemistry of the elements. Butterworth Heinemann, New York
2. Szasz L (1985) Pseudopotential theory of atoms and molecules. Wiley, New York
3. Gropen O (1988) The relativistic effective core potential method. In: Wilson S (ed) Methods in computational chemistry, vol 2. Plenum, New York
4. Breit G (1929) Phys Rev 34:553
5. Foldy LL, Wouthuysen SA (1950) Phys Rev 78:29
6. Cowan RD, Griffin DC (1976) J Opt Soc Am 66:1010
7. Sucher J (1980) Phys Rev A22:348
8. Lenthe E, van Baerends EJ, Snijders JG (1993) J Chem Phys 99:4597
9. Douglas M, Kroll NM (1974) Ann Phys (NY) 82:89
10. Hess BA (1986) Phys Rev A33:3742
11. Nakajima T, Hirao K (2000) Chem Phys Lett 329:511
12. Paulovic J, Nakajima T, Hirao K, Seijo L (2002) J Chem Phys 117:3597
13. Wolf A, Reiher M, Hess BA (2004) J Chem Phys 120:8624
14. Fraga S, Malli G (1968) Many electron systems: properties and interactions. Saunders, Philadelphia
15. Bethe HA, Salpeter EE (1977) Quantum mechanics of one- and two-electron atoms. Plenum, New York
16. Pyykkö P, Desclaux JP (1979) Acc Chem Res 12:276
17. Pyykkö P (2004) Angew Chem Int Ed 43:4412
18. Jensen G, Hess BA (1989) Z Phys D13:363
19. Witek HA, Nakajima T, Hirao K (2000) J Chem Phys 113:8015
20. Jaskólski W (1996) Phys Rep 271:1
21. Bielińska-Wąż D, Karwowski J, Saha B, Mukherjee PK (2003) Phys Rev E68:1
22. Kappes U, Schmelcher P (1995) Phys Rev A51:4542
23. Bielińska-Wąż D, Karwowski J, Diercksen GHF (2001) J Phys B34:1987
24. Sako T, Černušák I, Diercksen GHF (2004) J Phys B37:1091
25. Bielińska-Wąż D, Diercksen GHF, Klobukowski M (2001) Chem Phys Lett 349:215
26. Lo JMH, Klobukowski M (2004) Mol Phys 102:2511
27. Hess BA (1989) Phys Rev A39:6016
28. Wolf A, Reiher M, Hess BA (2002) J Chem Phys 117:9215
29. Nakajima T, Hirao K (2000) J Chem Phys 113:7786
30. Nakajima T, Yanai T, Hirao K (2002) J Comput Chem 23:847
31. Samzow R, Hess BA, Jensen G (1992) J Chem Phys 96:1227
32. Nakano H (1993) J Chem Phys 99:7983
33. Furlani TR, King HF (1985) J Chem Phys 82:5577
34. Fedorov DG, Finley JP (2001) Phys Rev A 64:042502
35. Witek HA, Fedorov DG, Hirao K, Viel A, P-O Widmark (2002) J Chem Phys 116:8396
36. Kellö V, Sadlej AJ (1996) Theor Chim Acta 94:93
37. Dunning TH (1989) J Chem Phys 90:1007
38. Witek HA, Finley JP, Choe YK, Hirao K (2002) J Comput Chem 23:957
39. Dunham JL (1932) Phys Rev 41:721
40. Schmidt MW, Baldridge KK, Boatz JA, Elbert ST, Gordon MS, Jensen JJ, Koseki S, Matsunaga N, Nguyen KA, Su S, Windus TL, Dupuis M, Montgomery JA (1993) J Comput Chem 14:1347
41. Pickering JC, Zilio V (2001) Eur Phys J D13:181
42. Bengtsson E, Olsson E (1931) Z Phys 72:163
43. Ringström U, Åslund N (1966) Ark Fys 32:19
44. Huber KP, Herzberg G (1979) Constants of diatomic molecules. Van Nostrand, New York
45. McLean AD (1983) J Chem Phys 79:3392
46. Balasubramanian K (1997) Relativistic effects in chemistry Part A, Chap. 5. Wiley-Interscience, New York
47. Ehrhardt JC, Davis SP (1971) J Opt Soc Am 61:1342
48. Pyykkö P (1988) Chem Rev 88:563
49. Sako T, Diercksen GHF (2003) J Phys B36:1681